Clinical & Translational Immunology

Australian and New Zealand Society for Immunology Inc.

Clinical & Translational Immunology 2020; e1168. doi: 10.1002/cti2.1168
www.wileyonlinelibrary.com/journal/cti

ORIGINAL ARTICLE

Hybrid Fc-fused interleukin-7 induces an inflamed tumor microenvironment and improves the efficacy of cancer immunotherapy

Ji-Hae Kim[1†], Young-Min Kim[1†], Donghoon Choi[2], Saet-byeol Jo[3], Han Wook Park[3], Sung-Wook Hong[4,5], Sujeong Park[3], Sora Kim[3], Sookjin Moon[3], Gihoon You[3], Yeon-Woo Kang[3], Yunji Park[3], Byung Ha Lee[2] & Seung-Woo Lee[1,3]

[1]Laboratory of Cellular Immunology, Department of Life Sciences, Pohang University of Science and Technology, Pohang, Korea
[2]Research Institute of NeoImmuneTech, Inc., Rockville, MD, USA
[3]Laboratory of Cellular Immunology, Division of Integrative Biosciences and Biotechnology, Pohang University of Science and Technology, Pohang, Korea
[4]Laboratory of T Cell Biology, Division of Integrative Biosciences and Biotechnology, Pohang University of Science and Technology, Pohang, Korea
[5]Department of Microbiology and Immunology, Center for Immunology, University of Minnesota Medical School, Minneapolis, MN, USA

Correspondence
S-W Lee, Laboratory of Cellular Immunology, Division of Integrative Biosciences and Biotechnology, Pohang University of Science and Technology, Pohang 37673, Korea.
E-mail: sw_lee@postech.ac.kr

[†]Equal contribution.

Received 12 February 2020;
Revised 7 July 2020;
Accepted 2 August 2020

doi: 10.1002/cti2.1168

Clinical & Translational Immunology
2020; **9**: e1168

Abstract

Objectives. Emerging oncotherapeutic strategies require the induction of an immunostimulatory tumor microenvironment (TME) containing numerous tumor-reactive $CD8^+$ T cells. Interleukin-7 (IL-7), a T-cell homeostatic cytokine, induces an antitumor response; however, the detailed mechanisms underlying the contributions of the IL-7 to TME remain unclear. Here, we aimed to investigate the mechanism underlying the induction of antitumor response by hybrid Fc-fused long-acting recombinant human IL-7 (rhIL-7-hyFc) through regulation of both adaptive and innate immune cells in the TME. **Methods.** We evaluated rhIL-7-hyFc-mediated antitumor responses in murine syngeneic tumor models. We analysed the cellular and molecular features of tumor-infiltrating lymphocytes (TILs) and changes in the TME after rhIL-7-hyFc treatment. Furthermore, we evaluated the antitumor efficacy of rhIL-7-hyFc combined with chemotherapy and checkpoint inhibitors (CPIs). **Results.** Systemic delivery of rhIL-7-hyFc induced significant therapeutic benefits by expanding $CD8^+$ T cells with enhanced tumor tropism. In tumors, rhIL-7-hyFc increased both tumor-reactive and bystander $CD8^+$ TILs, all of which displayed enhanced effector functions but less exhausted phenotypes. Moreover, rhIL-7-hyFc suppressed the generation of immunosuppressive myeloid cells in the bone marrow of tumor-bearing mice, resulting in the immunostimulatory TME. Combination therapy with chemotherapy and CPIs, rhIL-7-hyFc elicited a strong antitumor response and even under a T lymphopenic condition by restoring $CD8^+$ T cells. When combined with chemotherapy and CPIs, rhIL-7-hyFc administration enhanced antitumor response under intact andlymphopenic conditions by

restoring $CD8^+$ T cells. **Conclusion.** Taken together, these data demonstrate that rhIL-7-hyFc induces antitumor responses by generating T-cell-inflamed TME and provide a preclinical proof of concept of immunotherapy with rhIL-7-hyFc to enhance therapeutic responses in the clinic.

Keywords: immunotherapy, cytokine, interleukin-7, rhIL-7-hyFc, lymphopenia, tumor microenvironment

INTRODUCTION

Numerous types of non-neoplastic cells, including fibroblasts, endothelial cells, adipocytes and immune cells, are recruited within tumor masses into a complicated network of cells called the tumor microenvironment (TME).[1] The TME is classified as inflamed or non-inflamed depending on its immunostimulatory or immunosuppressive characteristics, respectively.[2] Prominent presence of immunosuppressive cells, such as $CD4^+Foxp3^+$ regulatory T (Treg) cells, tumor-associated macrophages (TAMs), and myeloid-derived suppressor cells (MDSCs), is a feature of a non-inflamed TME, which is associated with a poor prognosis among cancer patients.[3,4] Conversely, accumulation of effector cells, such as $CD8^+$ T cells, $CD4^+Foxp3^-$ T helper (Th) cells and natural killer (NK) cells, is associated with an inflamed TME, which is correlated with a favorable prognosis.[5] The TME has a dynamic immune status. The composition of intratumor immune cells can be changed by cells recruited from the blood and lymphatic circulation, and the functionality of tumor-infiltrated immune cells is influenced by neighbouring cells.[1] Hence, the induction of an inflammatory and immunostimulatory TME may enhance cancer immunotherapy approaches.

Among the effector subsets in the TME, $CD8^+$ tumor-infiltrating T lymphocytes (TILs) are the most crucial because they can specifically eliminate malignant cells by recognising tumor-specific antigens.[6] However, $CD8^+$ TILs often present T-cell exhaustion, which is generally observed in chronic viral infections and is characterised by sustained expression of immune-checkpoint molecules including PD-1, LAG-3 and TIM-3.[7] Thus, re-invigoration of exhaustion phenotypes of $CD8^+$ TILs is an important strategy for enhancing antitumor immune response. In fact, administration of checkpoint inhibitors (CPIs) reactivates $CD8^+$ TILs and suppresses tumor growth in preclinical and clinical settings.[8–11] Furthermore, cancer patients having a high frequency of $CD8^+$ T cells within tumors show better therapeutic outcomes against CPIs,[12] indicating that functional $CD8^+$ TILs are important for therapeutic responses. However, transient re-invigoration of exhausted T cells by CPIs and shortage of $CD8^+$ TILs in certain cancer types limit the success of cancer immunotherapy.[13,14]

The common gamma chain receptor family of cytokines, including interleukin-2 (IL-2), IL-4, IL-7, IL-9, IL-15 and IL-21, plays pleiotropic roles in T cells.[15] IL-7 is produced by stromal cells in lymphoid organs and plays essential roles in T-cell development, survival, and in the generation of memory T cells. IL-7 is particularly pivotal in restoring T-cell numbers under lymphopenic conditions by boosting homeostatic proliferation.[16] The potential antitumor effect of IL-7 has largely been evaluated in the development of cancer vaccines. Therein, ectopically expressed or exogenously administered IL-7 increases the survival and responses of vaccine-induced $CD8^+$ T cells during tumor challenge.[17,18] A recent study has also shown that the engineering of chimeric antigen receptor-T (CAR-T) cells expressing IL-7 improves antitumor activity.[19] Moreover, the administration of recombinant IL-7 (rIL-7) generates an antitumor response by expanding populations of CXCR3-expressing $CD8^+$ T cells.[20] Despite its promising antitumor effect, rIL-7 has a short half-life in serum, limiting its use as a cytokine-based drug. Hence, we developed a hybrid Fc-fused long-acting recombinant human IL-7 (rhIL-7-hyFc, efineptakin-alfa) with no cytotoxicity on target cells and a long half-life *in vivo*. Single topical treatment with rhIL-7-hyFc after administration of a DNA vaccine, which encodes tumor antigen, elicits antitumor responses by expanding populations of vaccine-induced tumor-specific $CD8^+$ T cells.[21] rhIL-7-hyFc is thus potentially applicable as a novel cytokine-based drug for

cancer immunotherapy; however, the mechanisms underlying rhIL-7-hyFc-mediated modulation of immune cells in the TME remain undetermined.

This study aimed to investigate the mechanism underlying the induction of antitumor response by rhIL-7-hyFc through the regulation of both adaptive and innate immune cells in the TME. We evaluated rhIL-7-hyFc-mediated antitumor responses in syngeneic tumor models, analysed the cellular and molecular features of TILs and changes in the TME after rhIL-7-hyFc treatment, and evaluated the antitumor efficacy of combination therapy of rhIL-7-hyFc and chemotherapy/CPIs.

RESULTS

Administration of rhIL-7-hyFc increases CD8$^+$ T cells and suppresses tumor growth

Recombinant human IL-7-hyFc is an engineered protein that has long bioavailability.[21,22] To investigate the systemic pharmacodynamic effects of rhIL-7-hyFc treatment, we subcutaneously (s.c.) administered a single dose of rhIL-7-hyFc and examined the immune compartments in the peripheral blood. rhIL-7-hyFc significantly increased CD3ε^+ T cells peaked at day 7, and the increment was remained up to day 12 (Figure 1a). B cells (B220$^+$), NK cells (NK1.1$^+$) and myeloid cells (CD11b$^+$) were also slightly increased between days 4 and 7 by rhIL-7-hyFc treatment; however, the increment was prominent in CD3ε^+ T cells (Supplementary figure 1a). Since IL-7 is a critical factor for the development and survival of T cells,[16] we next compared the effect of rhIL-7-hyFc treatment in between T-cell subsets. rhIL-7-hyFc augmented the number of both CD4$^+$ and CD8$^+$ T cells, but CD8$^+$ T cells, in particular, CD8$^+$CD44$^+$ subset showed the most prominent increase (Figure 1b). To further determine whether rhIL-7-hyFc changes the transcriptional profile of CD8$^+$ T cells, we next analysed the gene expression profile of CD8$^+$ T-cell subsets. On day 7, splenic CD8$^+$CD44$^-$ and CD8$^+$CD44$^+$ subsets were isolated from buffer- or rhIL-7-hyFc-treated mice, respectively, and their transcriptomic changes were analysed by RNA-sequencing. Compared with controls, rhIL-7-hyFc administration resulted in 108 differentially expressed genes (DEGs, defined as a fold change $\geq$ 1.5) (Figure 1c; Supplementary table 1). Among total DEGs, 43 and 42 DEGs were identified specific to CD8$^+$CD44$^-$ and CD8$^+$CD44$^+$ T-cell subsets, respectively, and 23 DEGs were found in both subsets (Supplementary figure 1b). Gene ontology analysis revealed that rhIL-7-hyFc treatment leads to the enrichment of genes related to the cell cycle/division and immune cell proliferation/differentiation in CD44$^-$ and CD44$^+$ subsets, respectively (Supplementary figure 1c). Meanwhile, genes that commonly changed in both subsets were highly enriched in regulating intracellular components associated with the mitotic process (Supplementary figure 1c). Collectively, rhIL-7-hyFc treatment mainly affected the expression of genes related to the cell cycle and cell division processes in CD8$^+$ T cells (Figure 1d). Interestingly, genes involved in chemokine signalling (*Ccl3, Ccl4, Ccl5, Ccr2* and *Cxcr3*) and effector functions (*Ifng, Gzmb* and *Gzmm*) were upregulated in only CD44$^+$ subset by rhIL-7-hyFc treatment (Supplementary figure 1d). These data suggest that rhIL-7-hyFc serves as a robust amplifier of CD8$^+$ T cells by affecting the transcriptional profiles associated with cell proliferation and immune response pathways.

Next, we investigated whether a single dose of rhIL-7-hyFc treatment could induce antitumor activity in murine syngeneic tumor models. MC-38 (colorectal carcinoma) cells were implanted, and then, rhIL-7-hyFc was treated s.c. when the tumors were palpable. rhIL-7-hyFc treatment significantly inhibited tumor growth compared with the buffer control in a dose-dependent manner (Figure 2a; Supplementary figure 2a). Consistent with the pharmacodynamic profile in naïve mice (Figure 1a and b), rhIL-7-hyFc predominantly expanded circulating CD8$^+$ T cells in the tumor-bearing mice (Figure 2b; Supplementary figure 2b). Because the tumor size was inversely correlated with the number of circulating CD8$^+$ T cells (Figure 2c), we next examined the role of CD8$^+$ T cells on the antitumor activity of rhIL-7-hyFc. Indeed, the antitumor efficacy of rhIL-7-hyFc was inhibited by CD8$^+$ T-cell depletion (Figure 2d). By contrast, NK cells played no role in the antitumor function of rhIL-7-hyFc. Notably, the depletion of CD4$^+$ T cells improved the antitumor efficacy of rhIL-7-hyFc (Figure 2d). rhIL-7-hyFc treatment expanded CD8$^+$ T cells far more in mice depleted of CD4$^+$ T cells than normal mice (data not shown). Furthermore, CD4$^+$ T-cell depletion could also remove CD4$^+$Foxp3$^+$ Treg cells. Therefore, we assume that a greater amplification of CD8$^+$ T cells and a deficit of Treg cells may result in a better

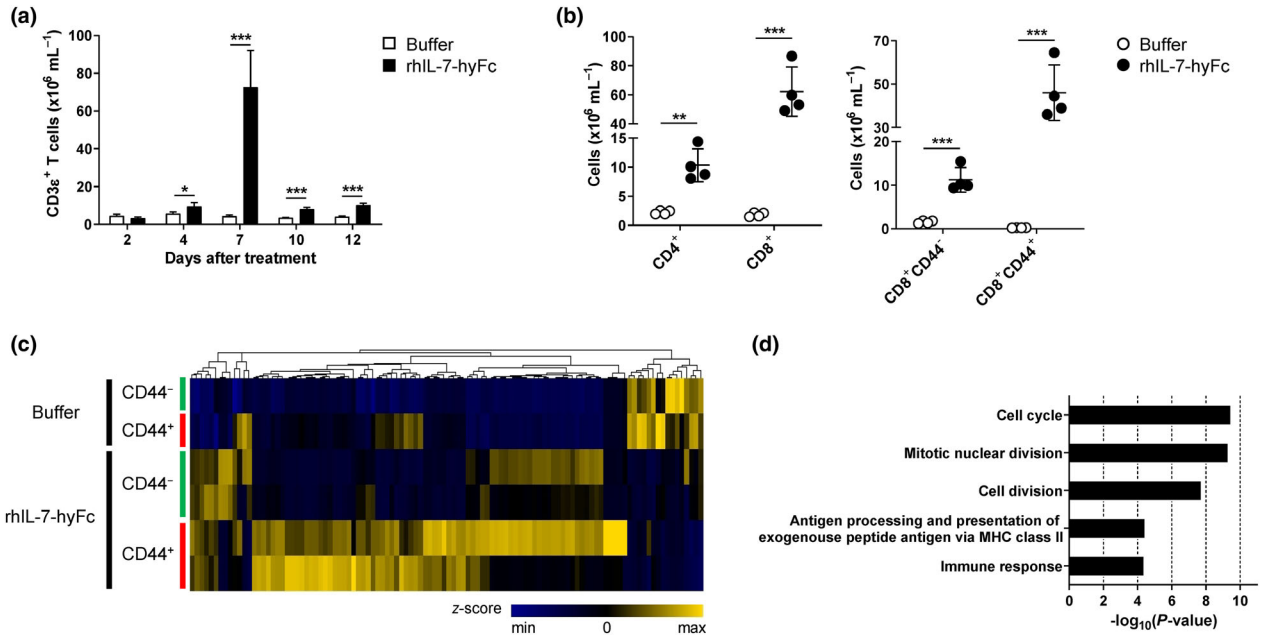

Figure 1. Hybrid Fc-fused long-acting recombinant human IL-7 (rhIL-7-hyFc) predominantly expands $CD8^+$ T cells and changes gene expression associated with cell proliferation. C57BL/6 mice were treated subcutaneously (s.c.) with 10 mg kg^{-1} of rhIL-7-hyFc or equal volume of buffer control. **(a, b)** Peripheral blood was collected, and cells were analysed by flow cytometry ($n = 4$ per group). **(a)** The number of $CD3\varepsilon^+$ T cells at indicated time points after treatment. **(b)** The number of $CD4^+$, $CD8^+$, $CD8^+CD44^-$ and $CD8^+CD44^+$ T cells on day 7 after treatment. **(c, d)** Splenic $CD8^+CD44^-$ and $CD8^+CD44^+$ T cells were isolated after 7 days of treatment, respectively, and analysed by RNA-sequencing. Gene expression was normalised as values of transcript per million mapped reads (FPKM) plus 1. Differentially expressed genes (DEGs) in each subset upon rhIL-7-hyFc treatment were defined as a fold change (log_2-transformed (FPKM plus1)) ≥ 1.5. **(c)** Heatmap of all 108 DEGs between buffer- and rhIL-7-hyFc-treated T subsets. Each row represents a DEG, and the colours represent the *z*-scores (FPKM plus 1) in the expression of a gene. **(d)** Gene ontology (GO) analysis of the DEGs described in **c** was performed by the DAVID database (v.6.8). The top 5 enriched GO terms associated with the biological process are shown. Data are shown as mean ± SD and representative of two independent experiments **(a, b)**. $*P < 0.05$; $**P < 0.01$; $***P < 0.001$.

antitumor efficacy by rhIL-7-hyFc in the absence of $CD4^+$ T cells. The antitumor response was also observed in mice having more established tumors (average of tumor sizes > 300 mm^3) by delayed treatment of rhIL-7-hyFc (Supplementary figure 2c). We further examined the antitumor efficacy of rhIL-7-hyFc treatment in two additional tumor models: CT-26 (colon carcinoma) and TC-1 (lung carcinoma). Consequently, the rhIL-7-hyFc treatment effectively inhibited tumor growth in mice bearing CT-26 or TC-1 tumors (Figure 2e). Overall, rhIL-7-hyFc effectively regulates tumor growth in solid tumor models, and the antitumor effect was mediated through a dose-dependent expansion of $CD8^+$ T cells.

rhIL-7-hyFc increases $CD8^+$ TILs having enhanced functions and tumor tropism

To understand how rhIL-7-hyFc-mediated antitumor response affects the immune compartments in tumors, we characterised TILs after treatment (Supplementary figure 3). Compared with buffer-treated control, both the frequency and the number of $CD8^+$ TILs markedly increased after rhIL-7-hyFc treatment whereas intratumoral NK cells remained unaltered (Figure 3a). Furthermore, $CD4^+Foxp3^-$ Th cells in rhIL-7-hyFc-treated tumors also increased while $CD4^+Foxp3^+$ Treg cells remained unaltered (Figure 3a); thus, rhIL-7-hyFc treatment increased the $CD8^+/Foxp3^+$ Treg ratio in the tumors (Figure 3b), which is a favorable prognostic indicator of antitumor immunity in mice and humans.[5] The marked expansions of $CD8^+$ TILs over Treg cells were also observed in other tumor models, CT-26 and TC-1 (Supplementary figure 4a and b). Furthermore, rhIL-7-hyFc enhanced the expression levels of Ki-67 and effector cytokines IFNγ and TNFα in $CD8^+$ TILs, while the proportion of granzyme B (GzmB)-expressing cells remained unaltered (Figure 3c–e).

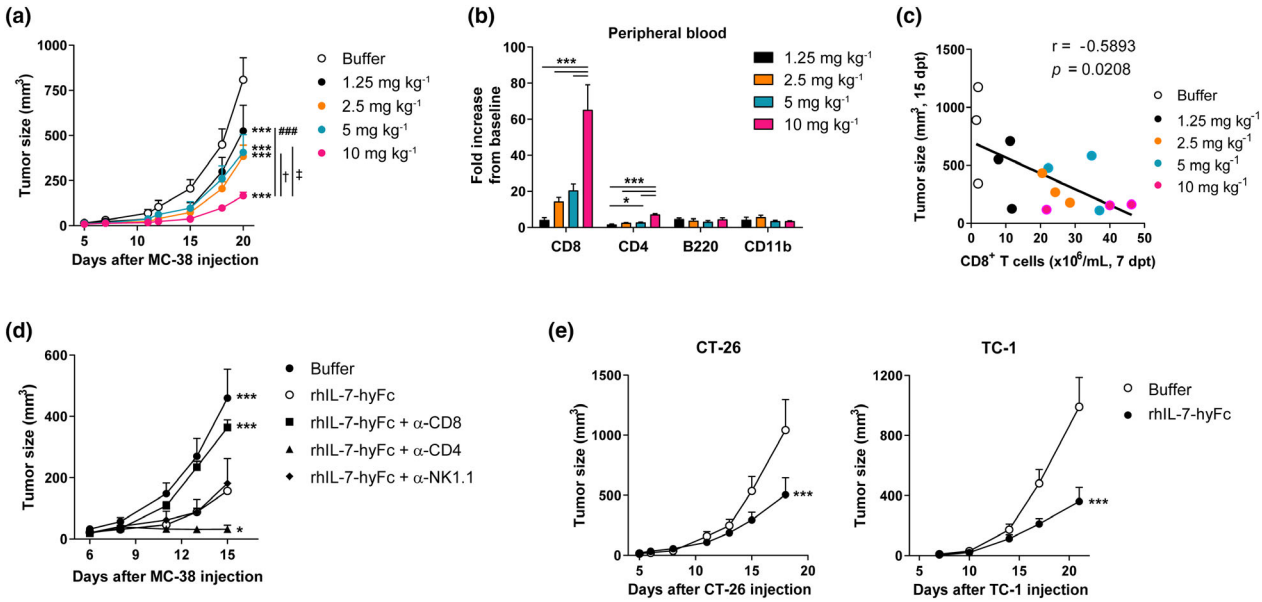

Figure 2. Hybrid Fc-fused long-acting recombinant human IL-7 (rhIL-7-hyFc) inhibits the growth of solid tumors through the expansion of $CD8^+$ T cells. **(a–c)** Mice bearing MC-38 tumors were treated s.c. with different doses of rhIL-7-hyFc on day 5. **(a)** Mean tumor growth curves (n = 5 or 6 per group). **(b)** Fold increases of peripheral blood $CD8^+$, $CD4^+$, $B220^+$ and $CD11b^+$ cells compared with baseline were quantified on day 7 after treatment (n = 3 per group). **(c)** A correlation was analysed between the number of $CD8^+$ T cells in peripheral blood mononuclear cells (PBMCs, 7dpt) and tumor size (15 dpt) (n = 3 per group). **(d)** Mice bearing MC-38 tumors were treated with rhIL-7-hyFc (10 mg kg^{-1}, s.c.) on day 5. Indicated monoclonal antibodies (200 μg $head^{-1}$) were treated intraperitoneally (i.p.) on 1 day before the rhIL-7-hyFc and every 3 days thereafter. Shown are mean tumor growth curves (n = 6 or 7 per group). **(e)** Mice bearing CT-26 (left, n = 5 or 6 per group) or TC-1 (right, n = 8 or 9 per group) tumors were treated with rhIL-7-hyFc (10 mg kg^{-1}, s.c.) on day 5 or day 1, respectively. Shown are mean tumor growth curves. Data are shown as mean ± SEM **(a, d, e)** or mean ± SD **(b)** and representative of 2 or 3 independent experiments. dpt; days post treatment, $^{*,\dagger,\ddagger}P < 0.05$; $^{***,\#\#\#}P < 0.001$.

An intact chemokine signalling is crucial for the recruitment of $CD8^+$ T cells into the TME. Indeed, CCR5 and CXCR3 are important receptors that dictate $CD8^+$ T-cell infiltration in tumor expressing CCL5, CXCL9 and CXCL10.[23] Thus, we sought to identify whether rhIL-7-hyFc contributes to chemokine/chemokine receptor pairs between the tumor bed and $CD8^+$ TILs. We found that most $CD8^+$ TILs were $CCR5^+$ and $CXCR3^+$ cells, whereas most $CD8^+$ T cells in the spleen were negative for both markers in mice bearing MC-38 tumors without treatment (Figure 3f). Consistent with the previous report, this result suggests that T cells are enriched in the tumor by chemotaxis. Interestingly, rhIL-7-hyFc treatment significantly increased $CD8^+$ T cells expressing both $CCR5^+$ and $CXCR3^+$ in spleens and tumors (Figure 3f and g). We also revealed that the mRNA expressions of cognate chemokines, *Ccl5*, *Cxcl9* and *Cxcl10*, were upregulated in rhIL-7-hyFc-treated tumors (Figure 3h), although only CCL5 increased at protein level (Figure 3i). These results indicate that rhIL-7-hyFc induces the expansion of circulating $CD8^+$ T cells having upregulated expression of chemokine receptors, thereby increases $CD8^+$ TILs. Taken together, these data suggest that rhIL-7-hyFc enhances the number and functional attributes of $CD8^+$ T cells which have upregulated tumor tropism.

rhIL-7-hyFc augments the number and function of tumor-reactive and bystander $CD8^+$ TILs

We further characterised the phenotype of $CD8^+$ TILs by assessing the markers associated with activation and differentiation. Based on the PD-1 expression, $CD8^+$ TILs can be classified into $PD\text{-}1^+$ versus $PD\text{-}1^-$ populations, which likely correspond to tumor-reactive versus bystander $CD8^+$ TILs, respectively.[24,25] In MC-38 tumors, the majority of $CD8^+$ TILs were $PD\text{-}1^+$ cells without treatment; however, administration of rhIL-7-hyFc elevated frequency of $PD\text{-}1^-$ cells compared with $PD\text{-}1^+$ cells among $CD8^+$ TILs (Figure 4a). Nonetheless, the number of both populations significantly increased by rhIL-7-hyFc treatment (Figure 4b). To further track down antigen-specific $CD8^+$ T cells,

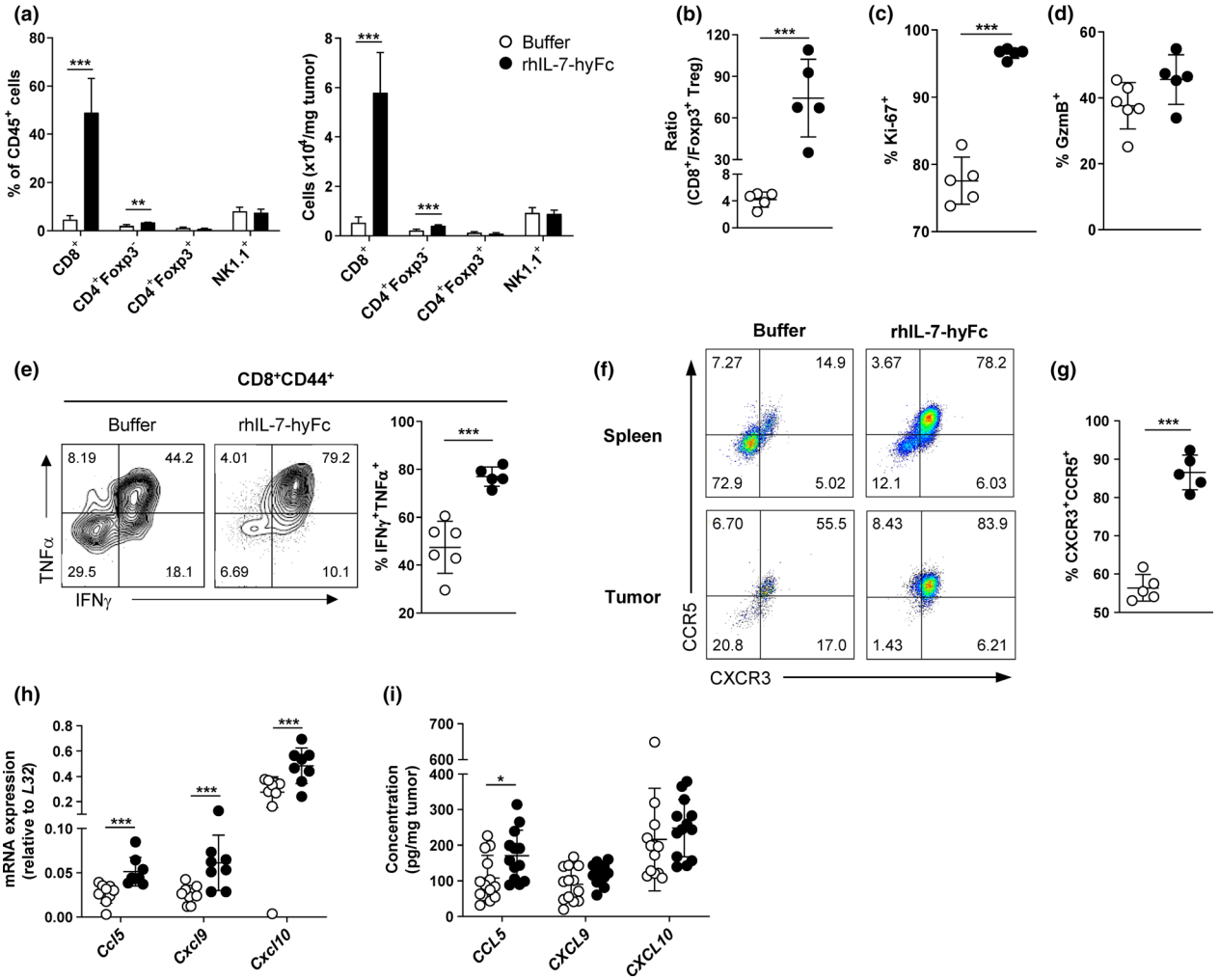

Figure 3. Hybrid Fc-fused long-acting recombinant human IL-7 (rhIL-7-hyFc) increases tumor-infiltrating CD8$^+$ T cells exhibiting enhanced functions and chemokine receptors. Mice bearing MC-38 tumors were treated with rhIL-7-hyFc (10 mg kg^{-1}, s.c.). **(a–e)** Cells from tumors were analysed on day 7 after treatment. **(a)** Frequency and the number of tumor-infiltrating lymphocytes (TILs) among CD45$^+$ cells. **(b)** Ratio of CD8$^+$ TILs to CD4$^+$Foxp3$^+$ Treg cells. **(c)** Frequency of Ki-67$^+$ cells in CD8$^+$ TILs. **(d)** Frequency of granzyme B (GzmB$^+$) cells in CD8$^+$ TILs. **(e)** Representative flow plots and frequency of IFNγ$^+$TNFα$^+$ cells in CD8$^+$CD44$^+$ TILs after PMA/ionomycin stimulation. **(f, g)** Cells were collected on day 7 after treatment from spleens and tumors. **(f)** Representative flow plots for the expression of CXCR3 and CCR5 on CD8$^+$ T cells. **(g)** Frequency of CXCR3$^+$CCR5$^+$ cells in CD8$^+$ TILs. **(h)** The mRNA levels of *Ccl5*, *Cxcl9* and *Cxcl10*. Levels were normalised to *L32*. **(i)** The protein levels of CCL5, CXCL9 and CXCL10. Levels were normalised to tumor weight (mg). Data are shown as mean ± SD and representative of 2 or 3 independent experiments (n = 5–13 per group per experiment). *P < 0.05; **P < 0.01; ***P < 0.001.

we utilised dextramer technology separating tumor antigen-specific cells among PD-1$^+$ tumor-reactive cells. The CD8$^+$p15E$^+$ TILs are tumor antigen-specific T cells detected by MHC-I dextramer loaded with p15E peptides harbouring a tumor-associated epitope derived from the endogenous murine leukaemia virus in MC-38 cells.[26] rhIL-7-hyFc treatment also upregulated the CD8$^+$p15E$^+$ TILs (Figure 4c).

Next, we evaluated the changes in the functional characteristics of CD8$^+$ TILs after rhIL-7-hyFc treatment. We wanted to compare the effects of rhIL-7-hyFc on each TIL subset, displaying the order of three subgroups from broad to a specific population (e.g. bystander → tumor-reactive → tumor antigen-specific population). Interestingly, rhIL-7-hyFc increased the frequency of GzmB$^+$ cells in PD-1$^-$ bystander TILs but not in PD-1$^+$ tumor-reactive and p15E$^+$ tumor antigen-specific TILs (Figure 4d and e). Instead, the production of cytokines, such as IFNγ and TNFα, was significantly elevated in

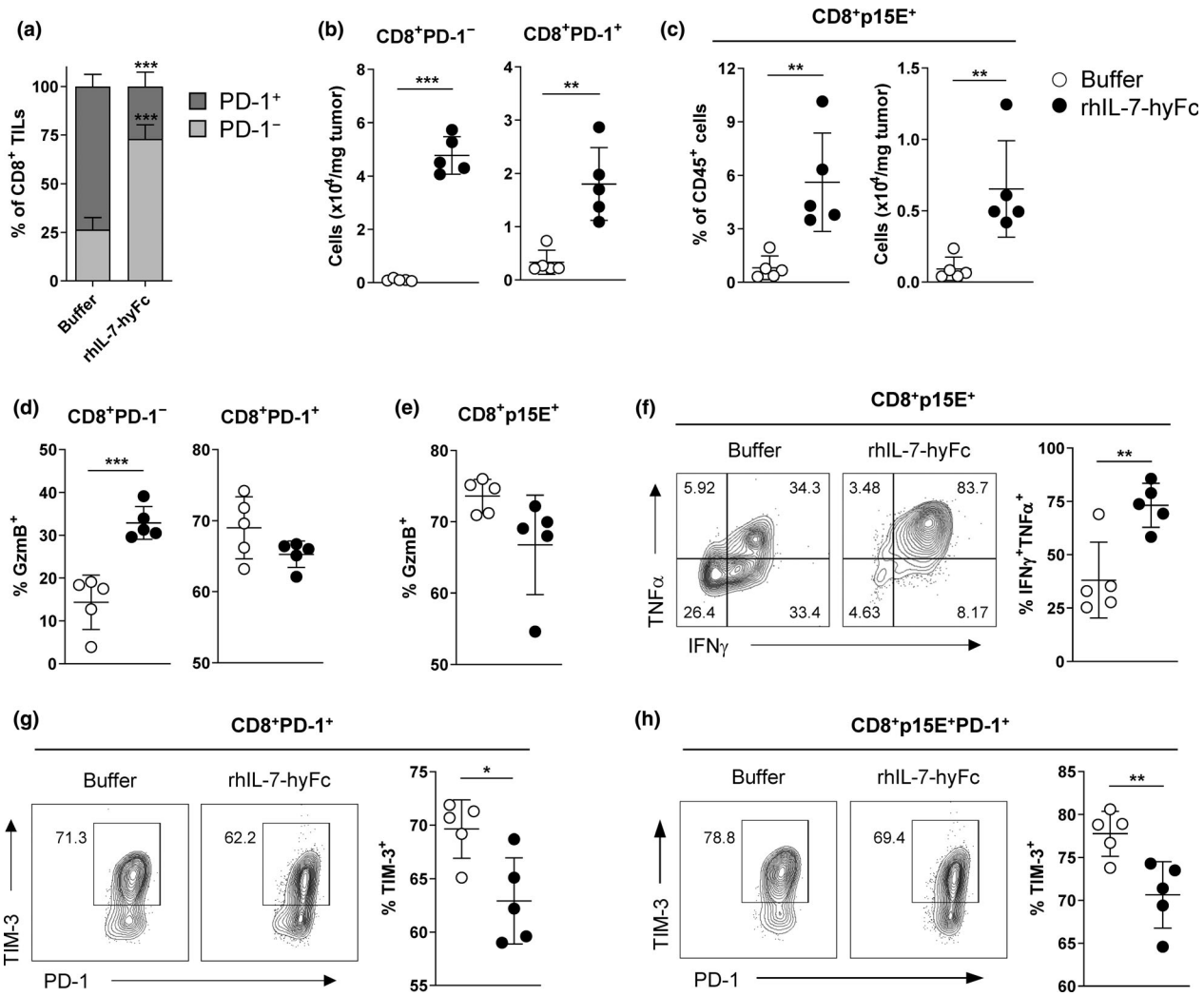

Figure 4. Hybrid Fc-fused long-acting recombinant human IL-7 (rhIL-7-hyFc) enhances the number and function of bystander and tumor-reactive $CD8^+$ TILs. Mice bearing MC-38 tumors were treated rhIL-7-hyFc (10 mg kg^{-1}, s.c.), and cells were collected on day 7 after treatment from tumors. **(a)** Frequency of $PD\text{-}1^+$ and $PD\text{-}1^-$ cells in $CD8^+$ TILs. **(b)** The number of $CD8^+PD\text{-}1^-$ (left) and $CD8^+PD\text{-}1^+$ (right) cells. **(c)** Frequency (left) and the number (right) of $CD8^+p15E^+$ cells. **(d)** Frequency of $GzmB^+$ cells in $CD8^+PD\text{-}1^-$ cells (left) and $CD8^+PD\text{-}1^+$ cells (right). **(e)** Frequency of $GzmB^+$ cells in $CD8^+p15E^+$ cells. **(f)** Representative flow plots and frequency of $IFN\gamma^+TNF\alpha^+$ cells in $CD8^+p15E^+$ cells after PMA/ionomycin stimulation. **(g, h)** Representative flow plots and frequency of $TIM\text{-}3^+$ cells in $CD8^+PD\text{-}1^+$ cells **(g)** and $CD8^+p15E^+PD\text{-}1^+$ cells **(h)**. Data are shown as mean ± SD and representative of 2 or 3 independent experiments (n = 5 per group). $^*P < 0.05$; $^{**}P < 0.01$; $^{***}P < 0.001$.

$p15E^+$ TILs by rhIL-7-hyFc treatment (Figure 4f). These results suggest that rhIL-7-hyFc augments the effector functions of $CD8^+$ TILs. Meanwhile, recent studies revealed that repeated antigen stimulation and immunosuppressive signalling elicit T-cell exhaustion, characterised by the expression of TIM-3.[27,28] To address the effect of rhIL-7-hyFc on the exhaustion status of $CD8^+$ TILs, we analysed TIM-3 expression on $PD\text{-}1^+$ tumor-reactive and $p15E^+PD\text{-}1^+$ tumor antigen-specific TILs. The frequencies of $TIM\text{-}3^+$ cells on both populations significantly decreased upon rhIL-7-hyFc treatment (Figure 4g and h). Collectively, rhIL-7-hyFc increases the populations of $CD8^+$ TILs with enhanced functions and reduced exhaustion.

rhIL-7-hyFc inhibits the development of myeloid-derived suppressor cells

A non-inflamed TME is characterised by the presence of immunosuppressive myeloid cells including MDSCs that consisting of two phenotypically different subsets: mononuclear MDSCs (M-MDSCs; $Ly6C^{hi}Ly6G^-$) and polymorphonuclear MDSCs

(PMN-MDSCs; $Ly6C^{lo}Ly6G^{+}$).[3] Hence, we investigated whether rhIL-7-hyFc affects the myeloid subsets in the TME (Supplementary figure 3). rhIL-7-hyFc significantly decreased $CD11b^{+}$ myeloid cells that compose approximately 75% of total $CD45^{+}$ cells in MC-38 tumors without treatment (Figure 5a). Concurrent with a previous report,[29] the majority of myeloid cells without treatment were MDSCs, with M-MDSCs dominating over PMN-MDSCs (Figure 5b). rhIL-7-hyFc treatment significantly reduced both M-MDSCs and PMN-MDSCs (Figure 5b). Therefore, the ratio of $CD8^{+}$/MDSCs significantly increased in the TME (Figure 5c), which is another positive indicator of the antitumor response.[30] Other myeloid subsets, including TAMs and dendritic cells (DCs), were identified in MC-38 tumors, and both populations were also decreased by rhIL-7-hyFc treatment (Supplementary figure 5a and b). Therefore, rhIL-7-hyFc has a universal effect suppressing most myeloid subsets in tumors. However, the far lower frequency of DCs was observed in tumors, and the extent of reduction in DCs by rhIL-7-hyFc was relatively minor compared with those of MDSCs and TAMs. Collectively, these results indicate that the myeloid population mostly affected by rhIL-7-hyFc in the TME is MDSCs.

Next, we determined how rhIL-7-hyFc reduces the populations of MDSCs in the TME by analysing changes in the factors involved in trafficking and induction of MDSCs. The levels of CCL2 and CXCL1, which are important chemokine signals to attract MDSCs into tumor sites,[31,32] remained unaltered in the tumors by rhIL-7-hyFc treatment, although *Ccl2* mRNA level was slightly increased (Figure 5d and e). Furthermore, the levels of colony-stimulating factor (CSF) family (such as *Csf1*, *Csf2* and *Csf3*), which are the growth factors for MDSCs, were comparable between groups (Figure 5f). We then investigated whether rhIL-7-hyFc affects the development of MDSCs in bone marrow (BM). The number of both $Ly6C^{hi}Ly6G^{-}$ and $Ly6C^{lo}Ly6G^{+}$ myeloid cells significantly decreased in the BM after rhIL-7-hyFc treatment (Figure 5g). Most myeloid cells do not express the IL-7 receptor alpha chain (IL-7Rα, CD127);[16] therefore, rhIL-7-hyFc may have indirectly affected the development of these cell populations. Indeed, rhIL-7-hyFc treatment downregulated $CD11b^{+}$ myeloid cells but upregulated $B220^{+}$ cells in the BM (Figure 5h), leading to the reduced ratio of myeloid to lymphoid cells in the BM (Figure 5i). These data suggest that haematopoiesis is skewed towards lymphopoiesis upon rhIL-7-hyFc treatment. Overall, our results indicate that rhIL-7-hyFc suppresses the accumulation of MDSCs in the TME by inhibiting the development of MDSCs in the BM. Furthermore, the adoptive transfer of MDSCs into tumor-bearing mice partially impeded the antitumor activity of rhIL-7-hyFc (Figure 5j), indicating that the reduction of immunosuppressive MDSCs is associated with the rhIL-7-hyFc-mediated antitumor response.

rhIL-7-hyFc improves the antitumor efficacy of chemotherapy and checkpoint inhibitor therapy

Given that rhIL-7-hyFc exerted antitumor responses via alteration of TME towards the T-cell-inflamed phenotype, we next investigated whether rhIL-7-hyFc enhances the antitumor activity of chemotherapy and CPIs. First, we evaluated the antitumor efficacy of rhIL-7-hyFc combined with cyclophosphamide (CPA), an alkylating agent used in chemotherapy for multiple cancers.[33] To protect the actively proliferating $CD8^{+}$ T cells in response to rhIL-7-hyFc by the cytotoxic effect of CPA, we set a therapeutic regimen to administer rhIL-7-hyFc after 2 days of CPA. The combination treatment of rhIL-7-hyFc with CPA enhanced the antitumor efficacy in comparison with monotherapy of each reagent (Figure 6a). Next, we proceeded to explore the antitumor efficacy of therapeutic regimens bringing rhIL-7-hyFc together with CPA and CPIs (α-PD-1, α-PD-L1 and α-CTLA-4). The triple combination regimens greatly enhanced the antitumor efficacy and survival rates, while combinations of CPA with CPIs without rhIL-7-hyFc generated minor antitumor efficacy compared with control (Figure 6b and c). Eradication of tumors was also found in some of the mice receiving triple combination regimens with α-PD-1 or α-CTLA-4 (Supplementary figure 6).

In the clinical setting, numerous cancer patients present with a reduced absolute lymphocyte count (ALC). This lymphopenic condition is considered a caution that the patients are poorly benefiting from CPI therapy.[34] Therefore, we next explored the antitumor effect of rhIL-7-hyFc under a long-term T-cell lymphopenic condition to mimic the clinical situation. We used thymectomised (Thx) mice with systemically decreased

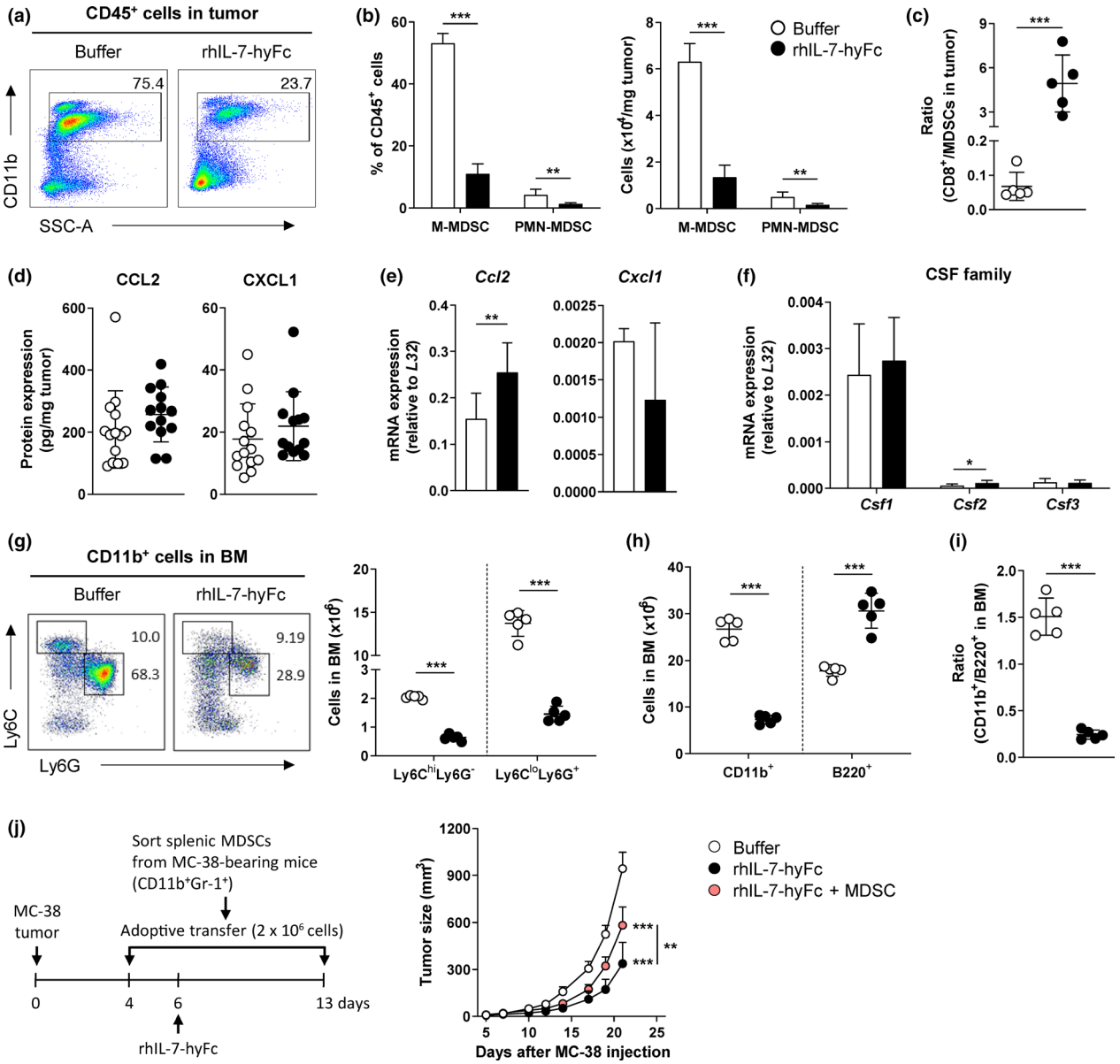

Figure 5. Hybrid Fc-fused long-acting recombinant human IL-7 (rhIL-7-hyFc) inhibits the development of myeloid-derived suppressor cells. **(a–i)** Mice bearing MC-38 tumors were treated rhIL-7-hyFc (10 mg kg^{-1}, s.c.), and cells were collected from tumors and bone marrow (BM) on day 7 after treatment. **(a)** Representative flow plots for the frequency of $CD11b^+$ myeloid cells in $CD45^+$ cells from tumors. **(b)** Frequency and the number of mononuclear myeloid-derived suppressor cells (M-MDSCs; $Ly6C^{hi}Ly6G^-$) and polymorphonuclear (PMN-MDSCs ($Ly6C^{lo}Ly6G^+$) in $CD45^+$ cells from tumors. **(c)** Ratio of $CD8^+$ TILs to MDSCs in tumors. **(d)** The protein levels of CCL2 and CXCL1. Levels were normalised to tumor weight (mg). **(e, f)** The mRNA levels of *Ccl2*, *Cxcl1* **(e)** and CSF family **(f)**. Levels were normalised to *L32*. **(g)** Representative flow plots for the frequency of MDSC subsets in $CD11b^+$ cells from the BM (left). The number of $Ly6C^{hi}Ly6G^-$ and $Ly6C^{lo}Ly6G^+$ cells in the BM (right). **(h)** The number of $CD11b^+$ and $B220^+$ cells in the BM. **(i)** Ratio of $CD11b^+$ to $B220^+$ cells in the BM. **(j)** The experimental scheme of MDSC transfer (left) and mean tumor growth curves (right). Data are shown as mean ± SD **(b–i)** or mean ± SEM **(j)** and representative of 2 or 3 independent experiments (n = 4–14 per group per experiment). *P < 0.05; **P < 0.01; ***P < 0.001.

populations of T cells (Supplementary figure 7a). Administration of rhIL-7-hyFc to these Thx mice also predominantly increased the number of $CD8^+$ T cells lasting more than 4 weeks after treatment (Supplementary figure 7b). The combination of rhIL-7-hyFc with α-PD-1 induced a considerable antitumor efficacy, while monotherapy with α-PD-1 showed no tumor suppression in the Thx mice

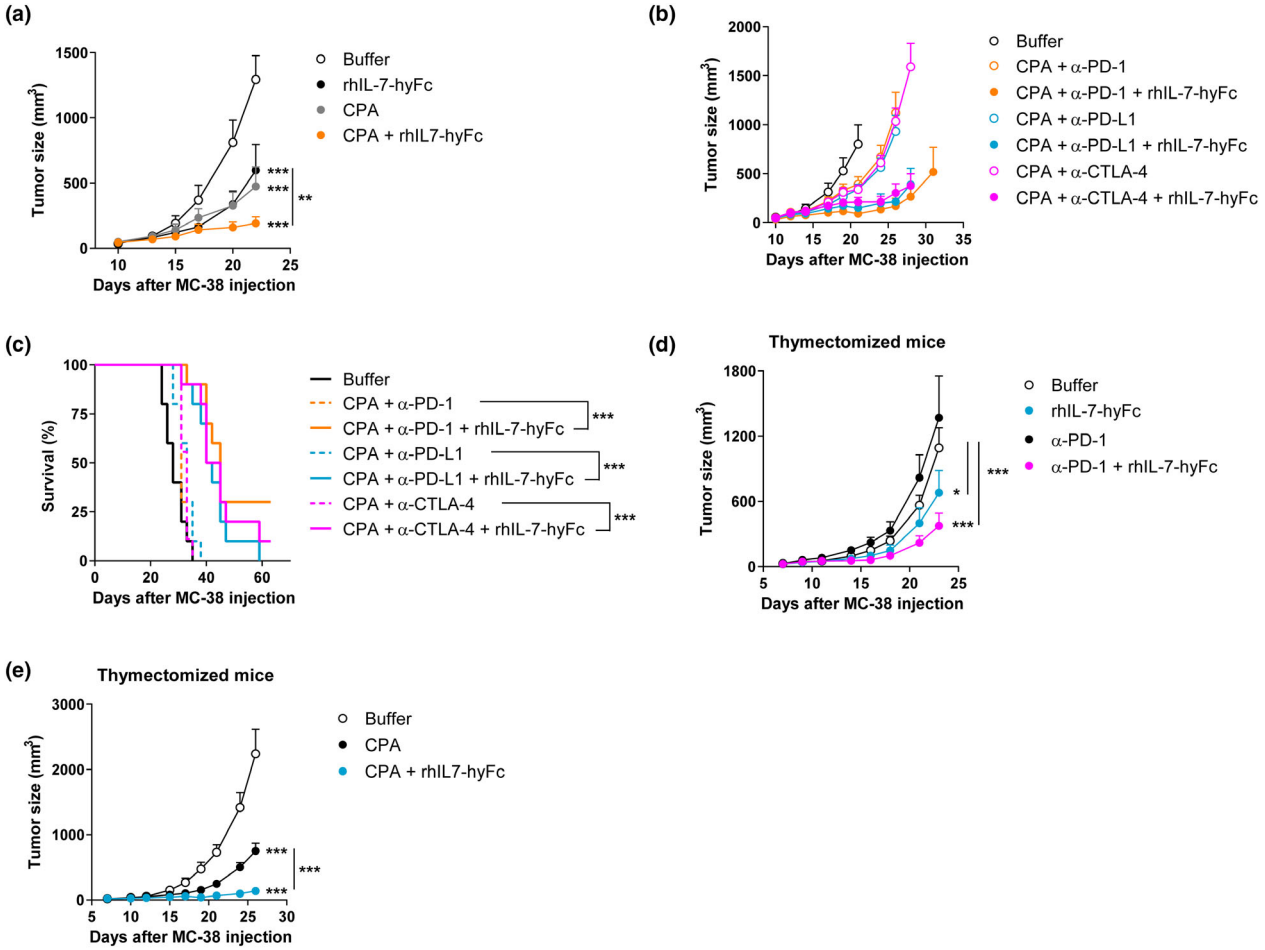

Figure 6. Hybrid Fc-fused long-acting recombinant human IL-7 (rhIL-7-hyFc) improves antitumor efficacy in combination with chemotherapy and checkpoint inhibitors. **(a)** Mice bearing MC-38 tumors were treated with rhIL-7-hyFc (10 mg kg^{-1}, s.c.) or CPA (100 mg kg^{-1}, i.p.) alone or in combination. Shown are mean tumor growth curves (n = 5 per group). **(b, c)** Mice bearing MC-38 tumors were treated with CPA and checkpoint inhibitor (CPI; 5 mg kg^{-1}, i.p.) or in combination with rhIL-7-hyFc (n = 9 or 10 per group). Mean tumor growth curves **(b)** and survival rates **(c)** are shown. **(d)** Thymectomised mice bearing MC-38 tumors were treated with rhIL-7-hyFc or α-PD-1 alone or in combination (n = 7–9 per group). Shown are mean tumor growth curves. **(e)** Thymectomised mice bearing MC-38 tumors were treated with CPA alone or in combination with rhIL-7-hyFc (n = 7 per group). Shown are mean tumor growth curves. Data are shown as mean ± SEM and representative of 2 or 3 independent experiments. *P < 0.05; **P < 0.01; ***P < 0.001.

(Figure 6d). Furthermore, rhIL-7-hyFc combined with CPA also elicited an enhanced antitumor efficacy as in the T-cell competent mice (Figure 6e). Collectively, rhIL-7-hyFc enhances antitumor activity through the combination with cytotoxic agents and immunotherapies, which work the same under conditions with a limited number of $CD8^+$ T cells.

DISCUSSION

Owing to the capacity of T-cell expansion without severe toxicity, exogenous administration of IL-7 has been considered a beneficial therapy for cancer patients;[35–39] however, antitumor responses and regulation of TME mediated by IL-7 treatment remain unknown. This study shows that systemic administration of rhIL-7-hyFc, a long-acting form of recombinant human IL-7, elicits antitumor effect through induction and maintenance of an inflamed and immunostimulatory TME (Figure 7).

Recombinant human IL-7-hyFc generates an antitumor response via the following mechanisms. First, rhIL-7-hyFc induces a drastic expansion of functional $CD8^+$ TILs with augmented expression of proliferation marker Ki-67 and the effector cytokines IFNγ and TNFα. Previous studies have

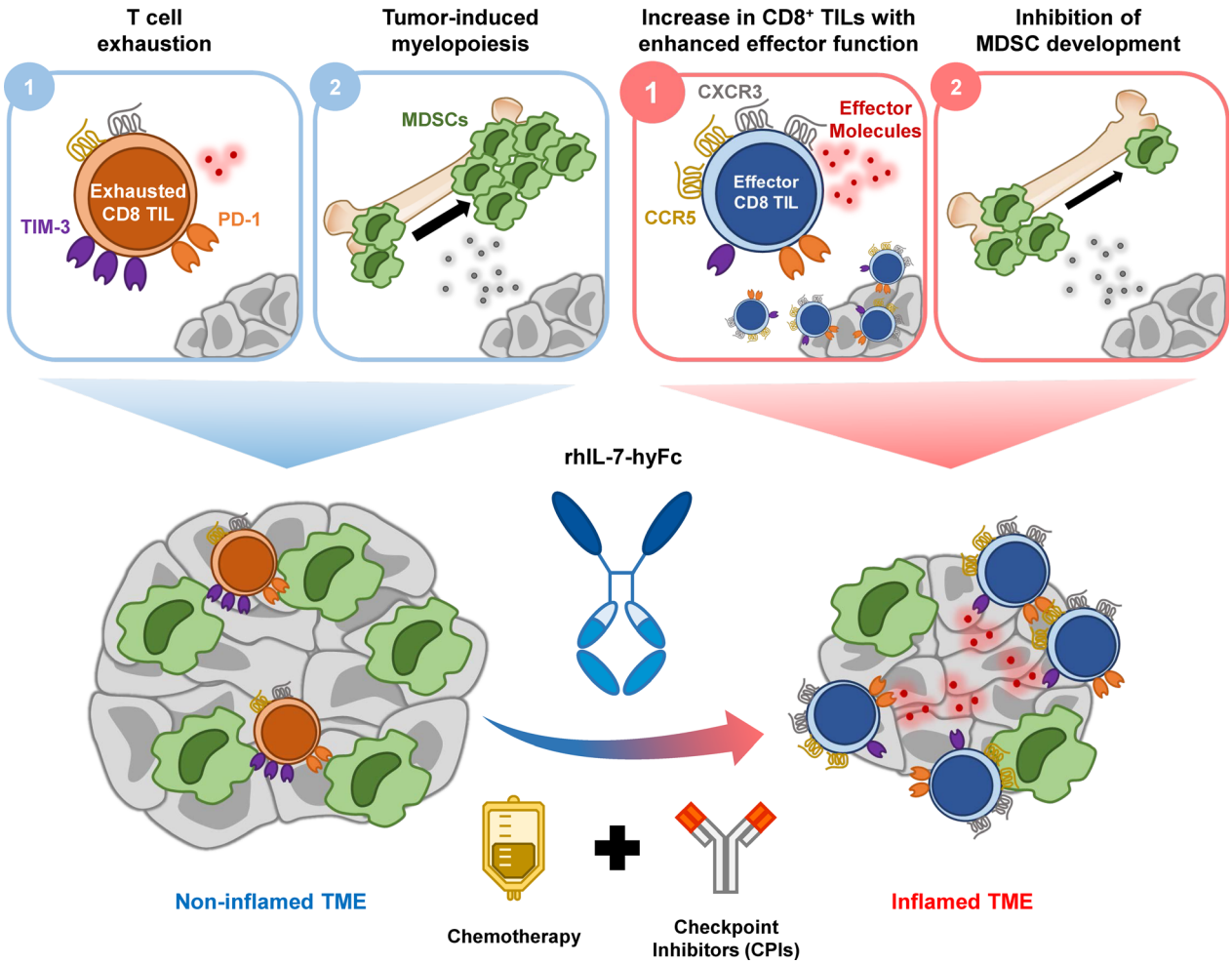

Figure 7. Hybrid Fc-fused long-acting recombinant human IL-7 (rhIL-7-hyFc) induces antitumor responses by promoting an inflamed TME. The tumor microenvironment (TME) is normally characterised as an immunosuppressive condition by the presence of exhausted $CD8^+$ TILs and regulatory immune cells such as MDSCs and Treg cells. A systemic administration of long-acting rhIL-7-hyFc promotes the expansion of $CD8^+$ TILs with less exhausted phenotype, while inhibiting the development of MDSCs, thereby converting an immunosuppressive TME into an inflamed one and controlling tumor growth. This unique activity of rhIL-7-hyFc improves the antitumor efficacy of standard chemotherapy and CPIs even under the T-cell lymphopenic condition by restoring T-cell counts, suggesting rhIL-7-hyFc as a potential new cytokine-based agent for cancer immunotherapy.

shown that exogenous IL-7 administration enhanced the infiltration of $CD8^+$ T cells expressing CXCR3 into tumors and the production of cognate ligands CXCL9 and CXCL10 in a murine lung carcinoma model.[20,40] Our results concur with the previous findings, in that rhIL-7-hyFc increased the proportion of CXCR3-expressing $CD8^+$ TILs. Furthermore, these $CD8^+CXCR3^+$ TILs co-expressed another chemokine receptor CCR5, and their expression was upregulated together with rhIL-7-hyFc treatment. Moreover, CCL5 was upregulated in the rhIL-7-hyFc-treated tumors. CCL5 is produced in both tumor cells and $CD8^+$ TILs in human ovarian cancer,[23] while the production of CXCL9 and CXCL10 is regulated by tumor cells and myeloid cell subsets.[23,41] Therefore, increased $CD8^+$ TILs upon rhIL-7-hyFc treatment may be responsible for the increase in CCL5. Collectively, rhIL-7-hyFc generates a large fraction of $CD8^+$ TILs with enhanced antigen responsiveness and tumor tropism. Meanwhile, rhIL-7-hyFc exerts minimal effects on the proliferation of $CD4^+$ T cells. These data are consistent with a previous report showing that chronic and excessive IL-7 preferentially induces the expansion of $CD8^+$ T cells but not $CD4^+$ T cells

because of the low availability of MHC class II required for $CD4^+$ T-cell expansion.[42] Collectively, rhIL-7-hyFc generates a large fraction of $CD8^+$ TILs with enhanced antigen responsiveness and tumor tropism.

Second, rhIL-7-hyFc increases both tumor-reactive, including tumor antigen-specific, and bystander $CD8^+$ TILs with enhanced functions. $CD8^+$ TILs in cancer patients are heterogeneous populations comprising a large proportion of bystander T cells and tumor-specific T cells.[43] In a chronic virus infection model, exogenous IL-7 greatly expands non-virus-specific bystander T cells that contribute to clearance of virus.[44] Concurrently, herein, rhIL-7-hyFc treatment predominantly expands $CD8^+$ TILs that do not express tumor-reactive marker PD-1. Furthermore, rhIL-7-hyFc promotes enhanced functions of the $PD\text{-}1^-$ bystander TILs by expressing elevated levels of cytotoxic molecule GzmB. Because bystander T cells might contribute to antitumor response in the inflamed TME,[45] re-directing the response of bystander T cells to eradicate tumors will be an effective means to reinforce the antitumor activity of rhIL-7-hyFc. Meanwhile, the number of tumor-reactive $CD8^+PD\text{-}1^+$ TILs was significantly increased by rhIL-7-hyFc treatment. Among the $PD\text{-}1^+$ TILs, rhIL-7-hyFc reduced the proportion of $TIM\text{-}3^+$ exhausted TILs. These data indicate that rhIL-7-hyFc may inhibit the differentiation of $PD\text{-}1^+$ TILs into exhausted T cells while augmenting the functionality of $CD8^+$ TILs. Since endogenously generated $CD8^+$ TILs are constantly influenced by the infiltration of newly produced T cells together with differentiation of themselves in tumor beds, the role of rhIL-7-hyFc in the exhausted T-cell subsets needs to be further elucidated. Nevertheless, our results show that rhIL-7-hyFc augmented the functions of $CD8^+$ TILs and reduced the exhausted phenotype, thereby inducing antitumor effect.

Finally, rhIL-7-hyFc reduces immunosuppressive MDSCs in tumors by inhibiting the early development of the cells from the BM. Together with Treg cells, MDSCs are major components of the immunosuppressive TME. During tumor progression, tumor-derived cytokines and growth factors facilitate tumor-induced myelopoiesis in the BM, leading to immunosuppression and tumor growth.[3] We found that rhIL-7-hyFc inhibits this tumor-induced myelopoiesis. It has been reported that progenitors of lymphoid and myeloid-lineage cells share their developmental niches in the BM,[46] and IL-7 promotes the expansion of lymphocyte progenitors. This suggests that rhIL-7-hyFc seems to upregulate lymphopoiesis at the expense of myelopoiesis in the BM, which leads to the reversion of the myeloid- to lymphoid-lineage cell ratio in the BM of mice treated with rhIL-7-hyFc. Collectively, rhIL-7-hyFc generates an inflamed and immunostimulatory phenotype of TME with the drastic expansion of functional $CD8^+$ T cells while decreases the immunosuppressive cells in the tumors. Based on this mechanism, we hypothesised that rhIL-7-hyFc can be positioned as a versatile partner to improve the efficacy of cancer therapy such as chemotherapy, CPIs, cancer vaccines and CAR-T-cell-based therapy.

As a T-cell amplifier, rhIL-7-hyFc may particularly benefit patients presenting a reduced number of $CD8^+$ T cells. Numerous cancer patients develop lymphopenia after conventional chemotherapy and radiotherapy,[47,48] and some patients present reduced ALC even before the treatments. Despite probable causality between lymphopenia and compromised anticancer immunity, it is still difficult to predict the outcomes of cancer therapy based on a personal background of T-cell profiles, including their number, functionality and diversity. However, recent reports have shown positive correlations between ALC and patient survival after cancer treatment.[49] Moreover, clinical benefits from CPI therapy depend on the ALC of the patient.[34] These results suggest that the absolute number of lymphocytes, such as that of $CD8^+$ T cells, is an important prognostic criterion to predict the efficacy of cancer immunotherapy. Accordingly, our results imply that rhIL-7-hyFc can enhance antitumor T-cell immune responses through combination therapeutic regimens, and the results obtained using Thx mice broadened the potential of rhIL-7-hyFc in clinical settings. Overall, this study shows that rhIL-7-hyFc is an important new cytokine-based drug in cancer immunotherapy. Recently, the data from a phase 1 clinical trial testing the effect of rhIL-7-hyFc in 30 healthy volunteers were published (ClinicalTrials.gov NCT02860715).[50] Briefly, rhIL-7-hyFc showed prolonged pharmacokinetics and increased ALC, mostly because of an increase in T cells, in peripheral blood of subjects. The trial also demonstrated that rhIL-7-hyFc treatment was safe and well-tolerated.[50] Most importantly, the worth of rhIL-7-hyFc (efineptakin-alfa) as a new cytokine drug for cancer immunotherapy should be evaluated

through ongoing clinical examinations (Clinical Trials.gov NCT04332653, NCT03687957, NCT03901573 and NCT02659800).

METHODS

Mice

C57BL/6N wild-type and BALB/c wild-type female mice (7–12 weeks) were purchased from the ORIENT BIO Inc. (Seongnam-si, Korea) and subsequently habituated under a specific pathogen-free condition at the animal facility of Pohang University of Science and Technology (POSTECH; Pohang-si, Korea). For thymectomy models, mice more than 8 weeks old were anaesthetised and surgically removed their thymus. All animal experiments were performed in accordance with National Institutes of Health guidelines for the care and approved by the Institutional Animal Care and Use Committee of the POSTECH (POSTECH-2016-0079-R2).

Cell lines

The murine colon carcinoma cell lines, MC-38 and CT-26, and the lung epithelial cell line, TC-1/luc, were kindly provided by Dr YC Sung (Genexine, Inc. Seongnam-si, Korea). MC-38 cells were cultured in Dulbecco's modified Eagle's medium (DMEM; Welgene, Gyeongsan-si, Korea). CT-26 and TC-1 cells were cultured in Roswell Park Memorial Institute medium 1640 (RPMI-1640; Welgene). Media were supplemented with 10% HyClone™ defined Fetal Bovine Serum (FBS; Cytiva, Marlborough, MA, USA) and Antibiotic-Antimycotic (Thermo Fisher Scientific, Waltham, MA, USA).

Tumor models and treatments

Recombinant human IL-7-hyFc and its formulation buffer were supplied by Research Institute of NeoImmuneTech, Inc. (Rockville, MD, USA) via Genexine, Inc. C57BL/6N or BALC/c mice were inoculated s.c. with 1×10^5 MC-38 or CT-26 cells, respectively. On day 5, mice were treated s.c. with 10 mg kg^{-1} rhIL-7-hyFc or the equivalent volume of formulation buffer as control. C57BL/6 mice were inoculated s.c. with 1×10^5 TC-1 cells and given 10 mg kg^{-1} rhIL-7-hyFc on the next day. For combination therapy, MC-38 tumors were grown for 10 days after inoculation. On day 10, mice were intraperitoneally (i.p.) given CPA (Endoxan®, CPA; Baxter, Deerfield, IL, USA; 100 mg kg^{-1}) and then rhIL-7-hyFc (10 mg kg^{-1}, s.c.) on day 12. Starting from day 16 after tumor inoculation, mice were injected i.p. with 5 mg kg^{-1} of anti-mouse PD-1 (clone 29F.1A12), anti-mouse PD-L1 (clone 10F.9G2), anti-mouse CTLA-4 (clone 9D9) or polyclonal rat IgG isotype control 5 times every 3 days. For cell depletion study, 200 μg of depleting antibodies was injected i.p. 1 day before rhIL-7-hyFc (s.c.) and every 3 days thereafter. The following antibodies were used for the cell depletion study: anti-mouse CD8α (clone 2.43); anti-mouse CD4 (clone GK1.5); anti-mouse NK1.1 (clone PK136); and rat IgG2b isotype control (clone LTF-2). All antibodies were purchased from BioXcell (Lebanon, NH, USA). Tumor size was calculated using the formula: 0.5 ab^2, where a as the longest diameter and b as the perpendicular diameter. Mice were euthanised when a exceeded 20 mm.

Cell preparation

Single-cell suspensions of BM cells were prepared by flushing the leg bones (one tibia and one femur per mouse) with RPMI-1640 supplemented with 2% Newborn Calf Serum (NCS; Thermo Fisher Scientific) plus antibiotic-antimycotic. Single-cell suspensions of spleens were prepared by dissociating the tissues and filtered through a 40-μm cell strainer (SPL Life Sciences Co., Ltd. Pocheon-si, Korea). Peripheral blood was harvested, and complete blood count analysis was performed using VetScan® HM2 analyzer (Abaxis, Inc. Union City, CA, USA). Red blood cells (RBCs) were removed by using RBC lysing buffer (Sigma-Aldrich, Saint Louis, MO, USA). Peripheral blood mononuclear cells were collected using Histopaque®-1083 (Sigma-Aldrich). Tumors were weighed and dissected mechanically and then digested with 400 units mL^{-1} collagenase D (Sigma-Aldrich) and 200 μg mL^{-1} DNase I (Sigma-Aldrich).

Flow cytometry

Single-cell suspensions were stained with Ghost Dye™ Violet 510 (Tonbo Biosciences, San Diego, CA, USA) to exclude dead cells and subsequently stained with anti-mouse CD16/32 (BioLegend, San Diego, CA, USA) and fluorescence-conjugated antibodies. The following primary antibodies were used: CD45 (clone 30-F11), CD3ε (clone 145-2C11), TCRβ (clone H57-597), CD8α (clone 53-6.7), CD4 (clone RM4-5), CD44 (clone IM7), B220 (clone RA3-6B2), NK1.1 (clone PK136), CD11b (clone M1/70), Ly-6C (clone HK1.4), Ly-6G (clone 1A8), PD-1 (clone RMP1-30), TIM-3 (clone RMT3-23), CCR5 (clone HM-CCR(7A4)), CXCR3 (clone CXCR3-173), TER-119 (clone TER-119), Gr-1 (clone RB6-8C5), anti-human Granzyme B (clone GB11), IFN-γ (clone XMG1.2), TNF-α (clone MP6-XT22), Foxp3 (clone FJK-16s) and Ki-67 (clone SolA15). Antibodies were purchased from BD Biosciences (San Jose, CA, USA), Thermo Fisher Scientific, or BioLegend. For detection of tumor antigen-specific $CD8^+$ T cells, a PE-conjugated H-2Kb/KWPWFTTL dextramer (Immudex, Virum, Denmark) was used according to the manufacturer's protocol. A PE-conjugated H-2Db/RAHYNIVTF dextramer (Immudex) for HPV16 E7-specific $CD8^+$ T cells were used as a control. For detection of intracellular cytokines, cells were stimulated for 5 h with PMA (20 ng mL^{-1}; Sigma-Aldrich) and ionomycin (1 μg mL^{-1}, Sigma-Aldrich) in the presence of GolgiStop™ and GolgiPlug™ (BD Biosciences). For staining of intracellular cytokines and chemokine receptors, cells were fixed/permeabilised with Cytofix/Cytoperm™ solution (BD Biosciences) or Foxp3/Transcription factor staining buffer set (Thermo Fisher Scientific) according to the manufacturer's protocols. Samples were acquired by LSRFortessa, LSRFortessa X-20 and FACSCanto II cytometers (BD Biosciences) and analysed with FlowJo software (Tree Star, Ashland, OR, USA).

RNA extraction and real-time quantitative PCR

Tumor tissues were mechanically homogenised in TRIzol reagent (Thermo Fisher Scientific). RNA was isolated using TRIzol–chloroform extraction according to the manufacturer's protocol. Quantitative PCR (qPCR) was performed for the gene expressions of *Cxcl1*, *Ccl2*, *Ccl5*, *Cxcl9*, *Cxcl10*, *Csf1*, *Csf2* and *Csf3* using QuantiTect Reverse Transcription kit (Qiagen, Hilden, Germany). The target gene expression was normalised to the level of *L32* gene expression. Primers are listed in Supplementary table 2.

RNA-sequencing analysis

For RNA sequencing, single-cell suspensions of spleens were prepared from mice treated with rhIL-7-hyFc (10 mg kg^{-1}, s.c.) or an equal volume of buffer control after 7 days of treatment. Cells were enriched by magnetic-activated cell sorting (MACS)-based separation using $CD8^+$ T-cell isolation kit (Miltenyi Biotec, Bergisch Gladbach, Germany) according to the manufacturer's protocol. Enriched $CD8^+$ T cells were further sorted into $CD8^+CD44^-$ and $CD8^+CD44^+$ subsets, respectively, under strict gating criteria of $CD44^{lo}$ and $CD44^{hi}$ populations using a Moflo-XDP Cell Sorter (Beckman Coulter Life Sciences, Indianapolis, IN, USA). RNA was isolated using TRIzol–chloroform extraction according to the manufacturer's protocol and shipped to Macrogen Inc. (Seoul, Korea). After quantity and quality check, RNA from three biological replicates of the buffer-treated group was pooled. Library construction and paired-end transcriptome sequencing were conducted using a HiSeq 4000 platform (Illumina Inc., San Diego, CA, USA) by Macrogen Inc. (Korea). Gene expression profile was normalised into values of fragments per kilobase of transcript per million mapped reads (FPKM) plus 1. The following groups were compared for the identification of differentially expressed genes (DEGs): buffer-treated $CD44^-$ vs. rhIL-7-hyFc-treated $CD44^-$ subsets, and buffer-treated $CD44^+$ vs. rhIL-7-hyFc-treated $CD44^+$ subsets. DEGs were defined as genes with a fold change [$\log_2$-transformed (FPKM plus 1)] $\geq$ 1.5. DEGs are listed in Supplementary table 1. The relative abundance of DEGs was clustered according to the *z*-score values of the FPKM plus 1 and visualised by heatmap using the R software (RStudio, Boston, MA, USA).

Chemokine analysis

Tumor tissues were harvested, weighed and then disrupted using a mechanical homogeniser in PBS. The protein levels of chemokines in tumor lysates were measured by using DuoSet and Quantikine ELISA kit (R&D Systems, Inc. Minneapolis, MN, USA) for mouse CXCL1 (DY453), CCL2 (DY479), CCL5 (DY478), CXCL9 (MCX900) and CXCL10 (MCX100) according to the manufacturer's instructions. Protein levels were normalised to tumor weights.

Adoptive cell transfer

For transfer of MDSCs, single-cell suspensions of spleens were prepared from mice bearing large established MC-38 tumors. Cells were then purified into $CD11b^+Gr\text{-}1^+$ subset using MACS (Miltenyi Biotec) according to the manufacturer's protocol. 2×10^6 sorted MDSCs were transferred intravenously into mice bearing MC-38 on days 4 and 13 of tumor inoculation. rhIL-7-hyFc (10 mg kg^{-1}, s.c.) was treated on day 6 of tumor inoculation.

Statistical analysis

The statistical analysis was assessed using Prism software (GraphPad Software, San Diego, CA, USA). The unpaired two-tailed *t*-test was used for a single comparison between two experimental groups. The one-way analysis of variance (ANOVA) with Bonferroni's post-test was used for multiple comparisons in the pharmacodynamics study. For tumor growth curves, the two-way ANOVA with Bonferroni's post-test was used for multiple comparisons; the statistical symbols were indicated on the last day of size measurement. For survival curves, the log-rank (Mantel–Cox) test was used. Correlations between tumor volumes and numbers of $CD8^+$ T cells in PBMCs were analysed by Spearman's correlation coefficient test. A *P*-value < 0.05 was considered statistically significant.

ACKNOWLEDGMENTS

We thank Man Kyu Ji and Yeon Kyung Oh (Genexine, Inc.) for supporting experiments. We thank Young Chul Sung (Genexine, Inc.) for helpful advice and providing cancer cell lines. We thank Jaehan Park and Se Hwan Yang (NeoImmuneTech, Inc.) for helpful advice and support, specifically the supply of rhIL-7-hyFc and its formulation buffer reagents. We thank Songa Lim and Haejin Jung for their technical assistance. We thank all members of the rhIL-7-hyFc science meeting from Genexine for helpful advice. This work was supported by the Bio & Medical Technology Development Program of the National Research Foundation (NRF) funded by the Korean government (MSIT) (2017M3A9C8033570), by BK21 Plus funded by the Ministry of Education, Korea (10Z20130012243), and by Research Institute of NeoImmuneTech, Inc.

CONFLICT OF INTEREST

DC and BHL are employees of the Research Institute of NeoImmuneTech, Inc., which supports rhIL-7-hyFc (the registered international nonproprietary name) and its formulation buffer reagents presented in this article. The remaining authors declare no conflict of interests.

AUTHOR CONTRIBUTIONS

Ji-Hae Kim: Conceptualization; Data curation; Formal analysis; Investigation; Methodology; Validation; Visualization; Writing-original draft; Writing-review & editing. **Young-Min Kim:** Conceptualization; Data curation; Formal analysis; Investigation; Methodology; Validation; Visualization; Writing-original draft; Writing-review & editing. **Donghoon Choi:** Data curation; Formal analysis; Funding acquisition; Investigation; Methodology; Resources; Writing-review & editing. **Saet-byeol Jo:** Formal analysis; Investigation;

Methodology; Validation; Writing-review & editing. **Han Wook Park:** Formal analysis; Investigation; Methodology; Validation; Writing-review & editing. **Sung-Wook Hong:** Investigation; Methodology; Writing-review & editing. **Sujeong Park:** Investigation; Methodology; Validation; Writing-review & editing. **Sora Kim:** Investigation; Methodology; Validation; Writing-review & editing. **Sookjin Moon:** Data curation; Visualization; Writing-review & editing. **Gihoon You:** Methodology; Writing-review & editing. **Yeon-Woo Kang:** Investigation; Visualization; Writing-review & editing. **Yunji Park:** Writing-review & editing. **Byung Ha Lee:** Conceptualization; Funding acquisition; Project administration; Resources; Writing-review & editing. **Seung-Woo Lee:** Conceptualization; Funding acquisition; Investigation; Project administration; Resources; Supervision; Writing-original draft; Writing-review & editing.

REFERENCES

1. Quail DF, Joyce JA. Microenvironmental regulation of tumor progression and metastasis. *Nat Med* 2013; **19**: 1423–1437.
2. Spranger S, Gajewski T. Rational combinations of immunotherapeutics that target discrete pathways. *J Immunother Cancer* 2013; **1**: 16.
3. Veglia F, Perego M, Gabrilovich D. Myeloid-derived suppressor cells coming of age. *Nat Immunol* 2018; **19**: 108–119.
4. Becht E, Giraldo NA, Dieu-Nosjean MC, Sautes-Fridman C, Fridman WH. Cancer immune contexture and immunotherapy. *Curr Opin Immunol* 2016; **39**: 7–13.
5. Fridman WH, Pages F, Sautes-Fridman C, Galon J. The immune contexture in human tumours: impact on clinical outcome. *Nat Rev Cancer* 2012; **12**: 298–306.
6. Finn OJ. Human tumor antigens yesterday, today, and tomorrow. *Cancer Immunol Res* 2017; **5**: 347–354.
7. Wherry EJ, Kurachi M. Molecular and cellular insights into T cell exhaustion. *Nat Rev Immunol* 2015; **15**: 486–499.
8. Zou W, Wolchok JD, Chen L. PD-L1 (B7–H1) and PD-1 pathway blockade for cancer therapy: Mechanisms, response biomarkers, and combinations. *Sci Transl Med* 2016; **8**: 328rv4.
9. Ribas A, Wolchok JD. Cancer immunotherapy using checkpoint blockade. *Science* 2018; **359**: 1350–1355.
10. Miller BC, Sen DR, Al Abosy R *et al*. Subsets of exhausted $CD8^+$ T cells differentially mediate tumor control and respond to checkpoint blockade. *Nat Immunol* 2019; **20**: 326–336.
11. Wei SC, Levine JH, Cogdill AP *et al*. Distinct cellular mechanisms underlie anti-CTLA-4 and anti-PD-1 checkpoint blockade. *Cell* 2017; **170**: 1120–1133.
12. Tumeh PC, Harview CL, Yearley JH *et al*. PD-1 blockade induces responses by inhibiting adaptive immune resistance. *Nature* 2014; **515**: 568–571.
13. Pauken KE, Sammons MA, Odorizzi PM *et al*. Epigenetic stability of exhausted T cells limits durability of reinvigoration by PD-1 blockade. *Science* 2016; **354**: 1160–1165.
14. Bonaventura P, Shekarian T, Alcazer V *et al*. Cold tumors: a therapeutic challenge for immunotherapy. *Front Immunol* 2019; **10**: 168.
15. Pulliam SR, Uzhachenko RV, Adunyah SE, Shanker A. Common gamma chain cytokines in combinatorial immune strategies against cancer. *Immunol Lett* 2016; **169**: 61–72.
16. Mackall CL, Fry TJ, Gress RE. Harnessing the biology of IL-7 for therapeutic application. *Nat Rev Immunol* 2011; **11**: 330–342.
17. Schroten-Loef C, de Ridder CM, Reneman S *et al*. A prostate cancer vaccine comprising whole cells secreting IL-7, effective against subcutaneous challenge, requires local GM-CSF for intra-prostatic efficacy. *Cancer Immunol Immunother* 2009; **58**: 373–381.
18. Pellegrini M, Calzascia T, Elford AR *et al*. Adjuvant IL-7 antagonizes multiple cellular and molecular inhibitory networks to enhance immunotherapies. *Nat Med* 2009; **15**: 528–536.
19. Adachi K, Kano Y, Nagai T, Okuyama N, Sakoda Y, Tamada K. IL-7 and CCL19 expression in CAR-T cells improves immune cell infiltration and CAR-T cell survival in the tumor. *Nat Biotechnol* 2018; **36**: 346–351.
20. Andersson A, Yang SC, Huang M *et al*. IL-7 promotes CXCR3 ligand-dependent T cell antitumor reactivity in lung cancer. *J Immunol* 2009; **182**: 6951–6958.
21. Choi YW, Kang MC, Seo YB *et al*. Intravaginal administration of Fc-fused IL7 suppresses the cervicovaginal tumor by recruiting HPV DNA vaccine-induced CD8 T cells. *Clin Cancer Res* 2016; **22**: 5898–5908.
22. Nam HJ, Song MY, Choi DH, Yang SH, Jin HT, Sung YC. Marked enhancement of antigen-specific T-cell responses by IL-7-fused nonlytic, but not lytic, Fc as a genetic adjuvant. *Eur J Immunol* 2010; **40**: 351–358.
23. Dangaj D, Bruand M, Grimm AJ *et al*. Cooperation between constitutive and inducible chemokines enables T cell engraftment and immune attack in solid tumors. *Cancer Cell* 2019; **35**: 885–900.
24. Gros A, Robbins PF, Yao X *et al*. PD-1 identifies the patient-specific $CD8^+$ tumor-reactive repertoire infiltrating human tumors. *J Clin Invest* 2014; **124**: 2246–2259.
25. Gros A, Parkhurst MR, Tran E *et al*. Prospective identification of neoantigen-specific lymphocytes in the peripheral blood of melanoma patients. *Nat Med* 2016; **22**: 433–438.
26. Zeh HJ 3rd, Perry-Lalley D, Dudley ME, Rosenberg SA, Yang JC. High avidity CTLs for two self-antigens demonstrate superior *in vitro* and *in vivo* antitumor efficacy. *J Immunol* 1999; **162**: 989–994.
27. Jin HT, Anderson AC, Tan WG *et al*. Cooperation of Tim-3 and PD-1 in CD8 T-cell exhaustion during chronic viral infection. *Proc Natl Acad Sci USA* 2010; **107**: 14733–14738.
28. Fourcade J, Sun Z, Benallaoua M *et al*. Upregulation of Tim-3 and PD-1 expression is associated with tumor antigen-specific $CD8^+$ T cell dysfunction in melanoma patients. *J Exp Med* 2010; **207**: 2175–2186.
29. Mosely SI, Prime JE, Sainson RC *et al*. Rational selection of syngeneic preclinical tumor models for immunotherapeutic drug discovery. *Cancer Immunol Res* 2017; **5**: 29–41.
30. Curran MA, Montalvo W, Yagita H, Allison JP. PD-1 and CTLA-4 combination blockade expands infiltrating T cells and reduces regulatory T and myeloid cells within B16 melanoma tumors. *Proc Natl Acad Sci USA* 2010; **107**: 4275–4280.

31. Qian BZ, Li J, Zhang H *et al*. CCL2 recruits inflammatory monocytes to facilitate breast-tumour metastasis. *Nature* 2011; **475**: 222–225.
32. Patel S, Fu S, Mastio J *et al*. Unique pattern of neutrophil migration and function during tumor progression. *Nat Immunol* 2018; **19**: 1236–1247.
33. Ahlmann M, Hempel G. The effect of cyclophosphamide on the immune system: implications for clinical cancer therapy. *Cancer Chemother Pharmacol* 2016; **78**: 661–671.
34. Diehl A, Yarchoan M, Hopkins A, Jaffee E, Grossman SA. Relationships between lymphocyte counts and treatment-related toxicities and clinical responses in patients with solid tumors treated with PD-1 checkpoint inhibitors. *Oncotarget* 2017; **8**: 114268–114280.
35. Rosenberg SA, Sportes C, Ahmadzadeh M *et al*. IL-7 Administration to humans leads to expansion of $CD8^+$ and $CD4^+$ cells but a relative decrease of $CD4^+$ T-regulatory cells. *J Immunother* 2006; **29**: 313–319.
36. Sportes C, Hakim FT, Memon SA *et al*. Administration of rhIL-7 in humans increases *in vivo* TCR repertoire diversity by preferential expansion of naive T cell subsets. *J Exp Med* 2008; **205**: 1701–1714.
37. Sportes C, Babb RR, Krumlauf MC *et al*. Phase I study of recombinant human interleukin-7 administration in subjects with refractory malignancy. *Clin Cancer Res* 2010; **16**: 727–735.
38. Tredan O, Menetrier-Caux C, Ray-Coquard I *et al*. ELYPSE-7: a randomized placebo-controlled phase IIa trial with CYT107 exploring the restoration of $CD4^+$ lymphocyte count in lymphopenic metastatic breast cancer patients. *Ann Oncol* 2015; **26**: 1353–1362.
39. Merchant MS, Bernstein D, Amoako M *et al*. Adjuvant immunotherapy to improve outcome in high-risk pediatric sarcomas. *Clin Cancer Res* 2016; **22**: 3182–3191.
40. .Andersson A, Srivastava MK, Harris-White M *et al*. Role of CXCR3 ligands in IL-7/IL-7Rα-Fc-mediated antitumor activity in lung cancer. *Clin Cancer Res* 2011; **17**: 3660–3672.
41. Chow MT, Ozga AJ, Servis RL *et al*. Intratumoral activity of the CXCR3 chemokine system is required for the efficacy of anti-PD-1 therapy. *Immunity* 2019; **50**: 1498–1512.
42. Guimond M, Veenstra RG, Grindler DJ *et al*. Interleukin 7 signaling in dendritic cells regulates the homeostatic proliferation and niche size of $CD4^+$ T cells. *Nat Immunol* 2009; **10**: 149–157.
43. Simoni Y, Becht E, Fehlings M *et al*. Bystander $CD8^+$ T cells are abundant and phenotypically distinct in human tumour infiltrates. *Nature* 2018; **557**: 575–579.
44. Pellegrini M, Calzascia T, Toe JG *et al*. IL-7 engages multiple mechanisms to overcome chronic viral infection and limit organ pathology. *Cell* 2011; **144**: 601–613.
45. Whiteside SK, Snook JP, Williams MA, Weis JJ. Bystander T cells: a balancing act of friends and foes. *Trends Immunol* 2018; **39**: 1021–1035.
46. Ueda Y, Kondo M, Kelsoe G. Inflammation and the reciprocal production of granulocytes and lymphocytes in bone marrow. *J Exp Med* 2005; **201**: 1771–1780.
47. Ellsworth SG. Field size effects on the risk and severity of treatment-induced lymphopenia in patients undergoing radiation therapy for solid tumors. *Adv Radiat Oncol* 2018; **3**: 512–519.
48. Grossman SA, Ellsworth S, Campian J *et al*. Survival in patients with severe lymphopenia following treatment with radiation and chemotherapy for newly diagnosed solid tumors. *J Natl Compr Canc Netw* 2015; **13**: 1225–1231.
49. Menetrier-Caux C, Ray-Coquard I, Blay JY, Caux C. Lymphopenia in cancer patients and its effects on response to immunotherapy: an opportunity for combination with cytokines? *J Immunother Cancer* 2019; **7**: 85.
50. Lee SW, Choi D, Heo M *et al*. hIL-7-hyFc, a long-acting IL-7, increased absolute lymphocyte count in healthy subjects. *Clin Transl Sci* 2020; e-pub ahead of print April 27 2020; https://doi.org/10.1111/cts.12800

Supporting Information

Additional supporting information may be found online in the Supporting Information section at the end of the article.